Structural, magnetic, and transport studies of La0.8MnO3 films

Q. Qian, T. A. Tyson, C. Dubourdieu, A. Bossak, J. P. Sénateur et al.

Citation: J. Appl. Phys. **92**, 4518 (2002); doi: 10.1063/1.1505667
View online: http://dx.doi.org/10.1063/1.1505667
View Table of Contents: http://jap.aip.org/resource/1/JAPIAU/v92/i8
Published by the AIP Publishing LLC.

Structural, magnetic, and transport studies of $La_{0.8}MnO_3$ films

Q. Qian and T. A. Tyson[a)]
Department of Physics, New Jersey Institute of Technology, Newark, New Jersey 07102

C. Dubourdieu, A. Bossak, and J. P. Sénateur
Laboratoire des Matériaux et du Génie Physique, CNRS UMR 5628, ENSPG BP46, 38402 St. Martin d'Hères, France

M. Deleon
Department of Physics, New Jersey Institute of Technology, Newark, New Jersey 07102

J. Bai
Oak Ridge National Laboratory, Oak Ridge, Tennessee 37831

G. Bonfait and J. Maria
Department of Chemistry, Nuclear and Technological Institute, P-2686 Sacavem Codex, Portugal

(Received 15 April 2002; accepted for publication 17 July 2002)

A study of the properties of $La_{0.8}MnO_3$ films of varying thickness was performed. Transport and magnetization measurements show that the ferromagnetic (metallic) volume fraction of the film varies from $\sim$ 1/4 for ultrathin 60 Å films to $\sim$ 1/2 for 1600 Å films. Multilength scale structural measurements reveal that near 300 Å, a transition from highly strained ultrathin films to relaxed bulk-like films occurs. The transition region is characterized by low surface roughness, high crystallite orientation, and broad *d*-spacing distributions. © *2002 American Institute of Physics.* [DOI: 10.1063/1.1505667]

I. INTRODUCTION

Due to the large (colossal) magnetoresistance (CMR) exhibited by perovskite manganites they have attracted a great deal of interest for the potential applications.[1] Many experiments have shown that the complex phase diagrams of CMR manganites are driven by the close interplay between the charge, spin, and orbital degrees of freedom in the system. It is evident the lattice strain plays an important role in the properties of these materials, which opens up the possibility of optimizing the properties of CMR oxides for specific applications by growing thin CMR films on substrates with different lattice spacings.[2,3]

The first systematic experimental study of the effect of thickness on the magnetotransport properties of thin films was performed by Jin *et al.*[2] which was later followed by others.[3,4] The characteristic feature found is that the metal-insulator (MI) transition is suppressed in very thin films. Systematic magnetic studies have also been performed.[5–9] J. O'Donnel *et al.*[9] suggested that the magnetic anisotropy in films seen in many experiments is dominated by strain induced anisotropy leading to an easy axis which occurs parallel to or normal to the film plane depending on substrate induced compression or tension.

The first attempt at quantifying the role of strain in these materials was made by Millis *et al.*[10] who showed that T_c is extremely sensitive to biaxial strain and that T_c reduction is quadratic in the Jahn-Teller (JT) distortion.[11] A local spin density calculation of the phase diagram of tetragonal manganites[12] showed that magnetic degrees of freedom can be indirectly controlled by lattice distortions via orbital degrees of freedom. It was argued that by changing the *c/a* ratio the e_g orbital extending along the elongated Mn–O bond is preferentially occupied.

In unannealed thin films of $La_{0.7}Ca_{0.3}MnO_3$ (< 250 Å) it is found that the peak resistivity temperature T_p decreases with film thickness while the Curie temperature T_C remains constant.[13] The difference between T_C and T_p is as large as 100 K for 50 Å films while the difference vanishes as in the case of bulk materials for films thicker than 250 Å. Consistent with these results, other studies have shown that ultrathin films (~ 50 Å) become insulators.[3,4] In addition, it is found that annealing of thin films has a rather striking effect—it converts insulating ultrathin films into metallic films[3,14] and increases the Curie temperature and saturation magnetization of thick films.[3,15]

To understand the effect of thickness and annealing on the properties of ultrathin manganite films we looked at three films (60, 300, and 1600 Å) of the ferromagnetic system $La_{0.8}MnO_3$. We examined the nanoscale structure by AFM measurements, the periodic structure by synchrotron x-ray diffraction and the local atomic structure by near-edge x-ray absorption spectroscopy. The AFM measurements reveal that the 60 Å film is composed of islands which coalesce into a smooth layer in the 300 Å film and lead to columnar growth in the 1600 Å film. The AFM and x-ray diffraction measurements reveal that near 300 Å, a transition from highly strained ultrathin films to relaxed bulk-like films occurs. X-ray absorption measurements reveal significant local distortions occur in the MnO_6 octahedra of the 60 Å film (more distorted than $LaMnO_3$) while the differences between the 300 and 1600 Å films are small. The results significantly expand our earlier study of these films[16] and fill in significant details.

[a)]Electronic mail: tyson@adm.njit.edu

TABLE I. X-ray diffraction of $La_{0.8}MnO_3$.

Index		0 0 4			0 4 0				4 0 0			
thickness (Å)	2Θ (deg.)	Width(deg.)	d(Å)	ε%	2Θ (deg.)	Width(deg.)	d(Å)	ε%	2Θ (deg.)	Width(deg.)	d(Å)	ε%
60	45.737(A)	0.57	1.982(23)	2.75	68.791(B)	1.00	1.363(17)	−1.37	69.178(B)	0.92	1.357(16)	−1.81
	46.267(B)[a]	0.90	1.961(36)	1.66	69.364(A)[a]	0.64	1.353(11)	−2.10	69.735(A)[a]	0.30	1.347(5)	−2.53
300	46.462(A)	0.41	1.953(16)	1.24	67.933(B)[a]	0.82	1.378(15)	−0.29	68.132(B)[a]	0.95	1.375(17)	−0.51
	46.710(B)[a]	0.27	1.943(11)	0.73	68.544(A)[a]	0.63	1.368(11)	−1.01	68.589(A)[a]	0.54	1.367(9)	−1.09
	47.241(C_2')	0.17	1.922(7)	−0.36	69.572(C_2)	0.57	1.350(10)	−2.32	69.535(C_2)	0.78	1.351(13)	−2.24
	45.830(C_2)		1.978	2.54								
1600	46.998(A)	0.31	1.932(12)	0.16	67.737(B)[a]	0.50	1.382(9)	0	67.731(B)[a]	0.52	1.382(9)	0
	47.076(B)[a]	0.12	1.929(5)	0	68.388(A)[a]	0.44	1.370(8)	−0.86	68.375(A)[a]	0.45	1.371(8)	−0.80

[a]Dominant peaks.

II. EXPERIMENTAL METHODS

Epitaxial $La_{1-x}MnO_3$ ($x \sim 0.8$) films were grown on (012) $LaAlO_3$ [referred to as $LaAlO_3$ (001) by the pseudocubic designation] substrates by metalorganic chemical vapor deposition. A liquid-injection delivery scheme[17–19] was used with a single liquid source. The β-diketonates La(tmhd)$_3$ and Mn(tmhd)$_3$ were dissolved together in 1,2 dimethoxyethane solvent. The reactor and the experimental procedure are described elsewhere.[17] Deposition runs were carried out at 700 °C under a total pressure of 0.67 kPa and an oxygen partial pressure of 0.33 kPa. After deposition, the films were *in situ* annealed in one atmosphere of oxygen at 800 °C for 15 min. Films of thickness 1600, 300, and 60 Å were prepared. The thickness was *in situ* monitored by a laser reflectometry setup. The growth rate was ~2 Å injection with an injection rate of 1 Hz. In the discussions below we index the $La_{1-x}MnO_3$ film with an orthorhombic structure with a doubled cell.

Preliminary magnetization measurements were performed in the range 4.2–320 K under a total magnetic field of 0.2 T in a vibrating sample magnetometer. The T_c values for the films were 180, 230, and 240 K for the 60, 300, and 1600 Å films, respectively. The final magnetization measurements were performed with a Quantum Design MPMS-XL SQUID magnetometer in a 0.2 T field and both measurements were performed with the magnetic field in the plane of the sample. For the 1600 Å film, magnetization measurements at 1.0 and 0.0020 T were also performed. Resistivity measurements were performed using a 4-point probe technique. The T_p (peak resistivity) values for the films were 225, 255, and 260 K for the 60, 300, and 1600 Å films, respectively. All films were found to be metallic. A Digital Instruments AFM NanoScope IIIa operating in contact mode was used to investigate the surface morphology. Synchrotron XRD experiments were performed on the Oak Ridge National Laboratory X-Ray beamline X14A at the National Synchrotron Light Source (NSLS) at the Brookhaven National Laboratory (BNL). The x-ray energy was set to 8.0468 keV ($\lambda = 1.5406$ Å). The measured diffraction peaks were fit by Gaussian functions and the results are given in Table I. $\varepsilon = (d - d_{1600})/d_{1600}$ is the degree of strain relative to the 1600 Å film B layer. Mn K-edge absorption spectra in fluorescence mode were measured on NSLS beamline X19A. Measurements were made for films with the beam electric field vector nearly 45° to the surface. The near-edge spectra were area normalized.

III. RESULTS

A. AFM, transport, and magnetization measurements

Figure 1 shows the atomic force microscopy images of the (a) 60 Å, (b) 300 Å, and (c) 1600 Å films plotted on the same scale. We can see that the 60 Å is not uniform but is composed of islands of $La_{0.8}MnO_3$. The islands become connected in the 300 Å film followed by columnar growth seen in the 1600 Å film. Interestingly, the 300 Å film is the most smooth film. Hence as a function of thickness different growth mechanisms prevail. It may be expected that the island structure would result in insulating films. However, these annealed films are found to be metallic.

In Fig. 2(a) we show the resistivity for the 60 and 1600 Å films. Note that both films show typical insulator-metal transition with metallic behavior at low temperature. Our magnetization measurements also show that the films have finite magnetic moments [Fig. 2(b)]. We point out that the magnetization of both films is significantly lower than the theoretical limit of 3.4 μ_B/Mn ion (on average) particularly in the 60 Å. For the 1600 Å film, measurements at 5 K at 1.0, 0.2, and 0.0020 T yielded moments of 1.5, 1.5, and 1.1 μ_B/Mn ion, respectively. The low moments found in the films are consistent with previous measurements on the La_xMnO_3 system.[20,21] The measurements suggest that ~1/2 of the 1600 Å film and ~1/4 of the 60 Å film volume is in the metallic state (assuming that only the metallic component is ferromagnetic). Since the film growth is different the decay of the strain as a function of thickness in unique to each film (Table I). In addition, the in-plane strain (with respect to the 1600 Å film) persists beyond 300 Å film.

B. X-ray diffraction measurements

Figures 3(a) and 3(b), show the diffraction profiles for two in-plane orthogonal reflections: (4 0 0) and (0 4 0). These measurements correspond to near 90° rotations relative to the (0 0 4) sample normal. Below, we call these reflections in-plane. For the 60 Å film (solid dots) a pair of lines (Table I) occurs at high angle (lower d spacing) relative

[a)]Electronic mail: tyson[@00ad]m.njit.edu

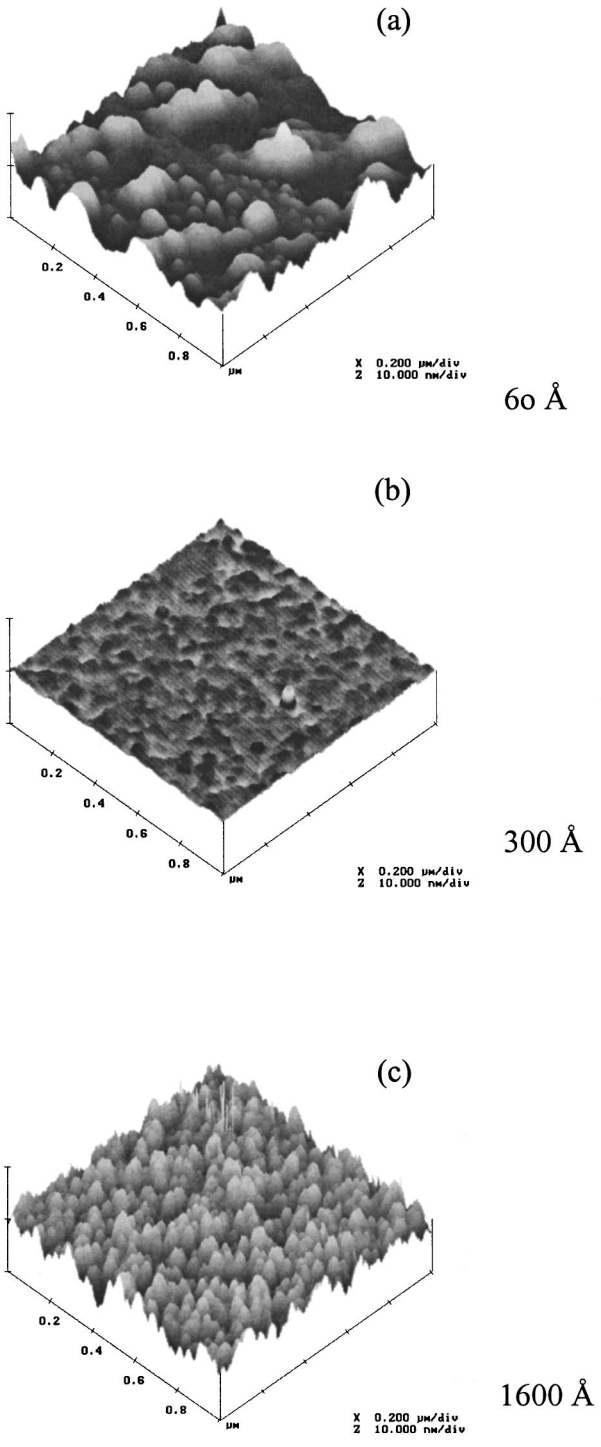

FIG. 1. Atomic force microscopy images of the (a) 60 Å, (b) 300 Å, and (c) 1600 Å films plotted on the same scale. Note the change in roughness with thickness.

to a pair lines found in the 1600 Å film (solid line) at lower angle (higher d spacing). While the corresponding pair of diffraction lines in the 300 Å film are significantly closer to those of the 1600 Å film than those of the 60 Å film. The 300 Å film has an additional peak (C_2) with d spacing similar to those of the 60 Å film. The substrate peak appears for all orientations at higher angle indicating that the substrate has a smaller lattice constant than the films. From ϕ scans, we find epitaxial growth in all of the films.

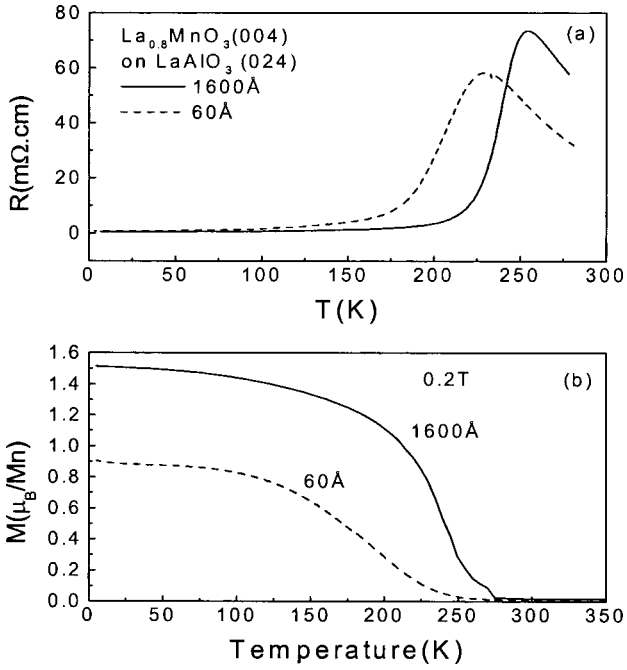

FIG. 2. (a) Resistivity and magnetization at (b) 0.2 T of the 60 (dashed line) and 1600 Å (solid line) films are shown as a function of temperature. Note that the saturation magnetization of 3.4 μ_B/Mn ion is not achieved.

In Fig. 3 one can see that the relative intensities of the two peaks are the same for the (400) and (040) scans. If the in-plane lattice were rectangular and we were observing rotated crystallites with two distinct in-plane lattice parameters, the intensities should reflect the thickness (in-plane) for a given direction in the crystallites. Rotation by 90° would result in the reversal of the peak intensities. This is not observed. This eliminates the possibility of two in-plane lattice parameters producing the double peak structure observed. Moreover, the relative intensities of the two peaks is not the same, ruling out the possibility of a 50/50 mixture of two rectangular cells. The two-peak structure is consistent

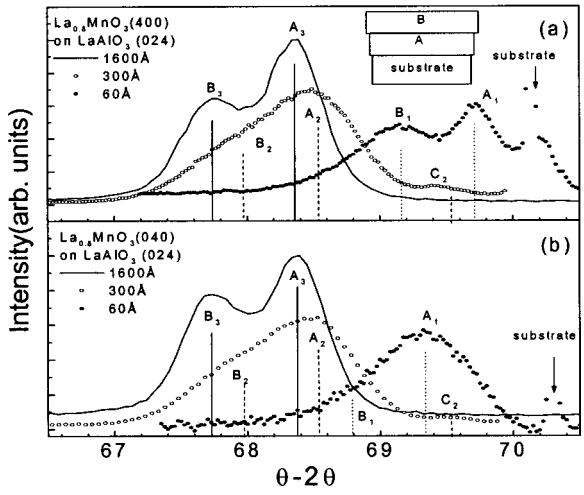

FIG. 3. X-ray diffraction θ-2θ scans of $La_{0.8}MnO_3$ film with the scattering plane approximately parallel and normal to surface. Diffraction peaks for (a) measurements along the direction (4 0 0) and (b) along the direction (0 4 0) are shown as two in-plane scans. Each pattern was fit by a set of Gaussian peaks and the vertical bars show the approximate peak positions (Table I).

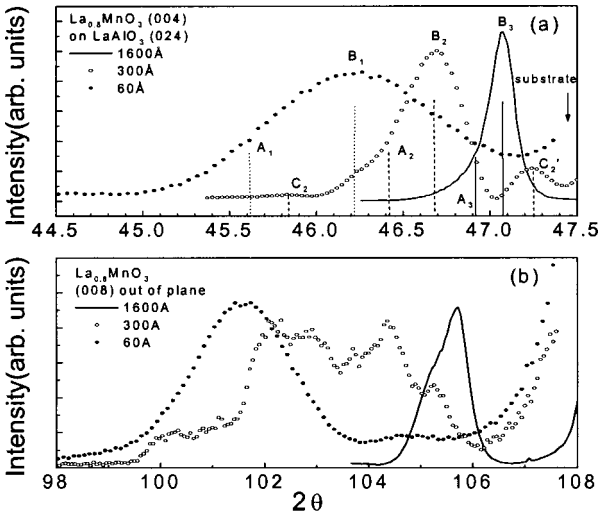

FIG. 4. Out-of plane (a) (0 0 4) scans and (b) (0 0 8) scans. The solid line, open dotted line, and closed dotted lines are for the 1600, 300, 60 Å films, respectively. Each pattern was fit by a set of Gaussian peaks and the vertical bars show the approximate peak positions (Table I). The 300 Å film in particular exhibits a distribution of *d* spacings.

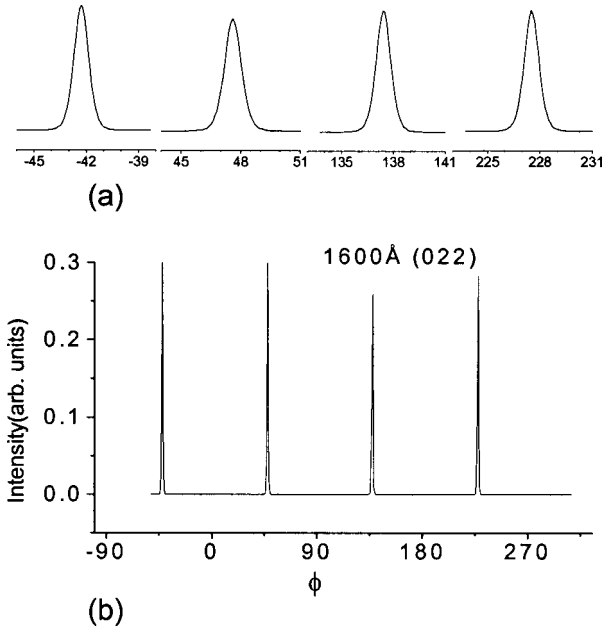

FIG. 5. ϕ scans about the (022) direction for the 1600 Å film; (a) shows the expanded region near the peaks and (b) shows the full scan.

with a film composed of two regions one near the substrate (A peaks) which is highly constrained by the substrate lattice and a more relaxed region away from the substrate (B peaks) with significant lattice relaxation (expansion). Hence, the 300 and 1600 Å films are composed of a strained A layer with a covering metallic B layer.

In the 60 Å film, the in-plane (400) and (040) reflections yield A layer spacings of 1.347 Å (the A_1 peak for (400)) and 1.353 Å [the A_1 peak for (040)], and B layer spacings of ~1.357 Å [peak B_1 for (400)] and 1.363 Å [peak B_1 for (040)]. That means that in very thin film there is in-plane asymmetry in both A and B layers. The 60 Å film tracks the substrate in-plane asymmetry as seen in the difference in the peak position for the substrate peaks. On the other hand the 300 and 1600 Å films reveal no such asymmetry [compare A_3 and B_3 for the (400) and (040) reflections in (a) and (b)] suggesting cubic symmetry as previously found in thick $La_{1-x}MnO_3$ films.

Figure 4 shows the out-of-plane diffraction profiles for the three films. In Fig. 4(a) the patterns at low angle are given. All profiles decomposed into ~two peaks except for the 300 Å films, which has at least four peaks with the addition of weak features labeled C_2 and C_2' at low and high angle, respectively. Apart from these weaker peaks, the peaks positions (A and B for all films) are quite consistent with the in-plane measurement if one assumes an approximately constant volume, if the film is compressed in-plane, it will relax (expand) out-of-plane. In this way, the corresponding peak labels found in the in-plane measurements are matched to the out-of-plane measurements. The only exception is peak C_2', which has no analog in the in-plane measurements but if we consider the broad profile on the low angle side of the 300 Å film in the in-plane scan, it is possible that a corresponding weak shoulder exists. The peak position widths and strain parameters are summarized in Table I.

The trend in Fig. 4(a) is followed by the high angle (008) scans with one significant exception. The 300 Å film reveals a weak (in terms of the origin total intensity) multicomponent distribution compared to the sharp peaks seen in for 60 and 1600 Å. The (008) can be considered a second order Bragg reflection which probes the same *d* spacing as the (004) reflection (since there are no atomic planes corresponding to $d_{004}/2$). The loss of long range order between the 60 and 1600 Å suggest that the 300 Å film is in a transition or crossover region moving away from the highly strained and substrate-like thin film (60 Å) and relaxing toward bulk-like properties exhibited by thick films (1600 Å). In fact, the (008) peak has components with position near the corresponding 60 and 1600 Å peak positions. Supporting this are the additional peaks, C_2 and C_2', seen in the (004) reflection for the 300 Å film.

ϕ scans about the (022) direction are shown for the 1600, 300, and 60 Å films in Figs. 5 through 7 (the reflection contains both the A and B components as in the out-of-plane scans); (a) shows the expanded region near the peaks and (b) shows the full scans. No structure was found in the peaks in the 300 and 1600 Å films. However, for the 60 Å films the peaks split into multiple components as a result of small differences in orientation between crystal grains. Note that the phi scale in Fig. 7(a) is 1/15 of that in Figs. 5(a) and 6(a). The widths of the peaks of the 60 Å film are significantly lower than those of the thicker films due to the high order imposed by the substrate. The split features in the phi scans of this thin film possibly reflect twinning of the $LaAlO_3$ substrate. The varying total intensities in Fig. 7(b) reflect the difficulty of maintaining the maximum for these narrow peaks.

Figure 8 shows θ-χ scans of the (004) planes of the (a) 1600, (b) 300, and (c) 60 Å films. The main observation is that the 300 Å film has the most well oriented crystal grains

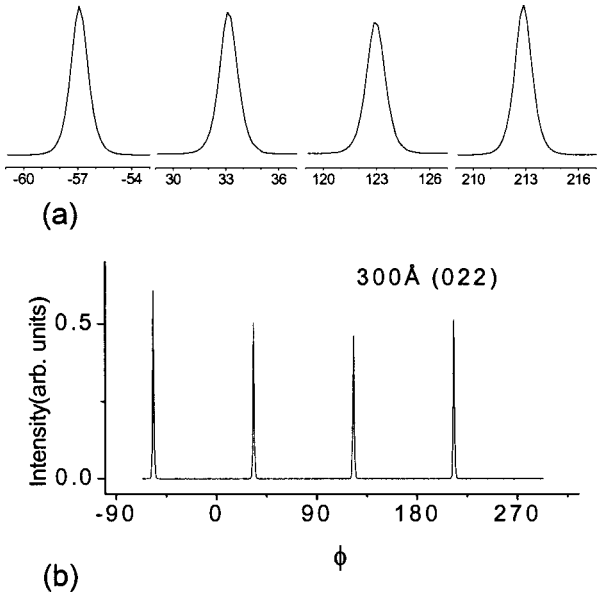

FIG. 6. ϕ scans about the (022) direction for the 300 Å film; (a) show the expanded region near the peaks and (b) shows the full scan.

(consistent with the AFM measurements). The vertical stacking of the atomic layers is highly ordered in the 300 Å film. This high degree of orientation is reduced by continued film growth (1600 Å) or substrate induced strain (for in the 60 Å).

C. Local structure measurements

Local structural information can be gleaned from x-ray absorption measurements. The main line corresponds to a 1*s* -4*p* transition on the Mn site. In octahedral symmetry (at the Mn site) there is no orientational dependence of the Mn main line. In reduced symmetry due to local distortions of the MnO_6 octahedra, the 4*p* peak will split into two or three components with progressive reduction in symmetry. Local distortions such as JT distortions produce such reductions in symmetry and generate orientational dependent splittings of the main line. In $LaMnO_3$ and other JT systems, broad main lines, and splitting have been predicted and measured.[22,23]

We measured Mn K-edge absorption spectra of these films [Fig. 9 (a)]. This spectrum shows a strong dependence of width of the 1*s*–"4*p*" peaks with thickness. The broadest and most narrow ones correspond to the 60 and 1600 Å films, respectively. We note that the 300 and 1600 Å have similar profiles while the 60 Å film is distinctly broader. In

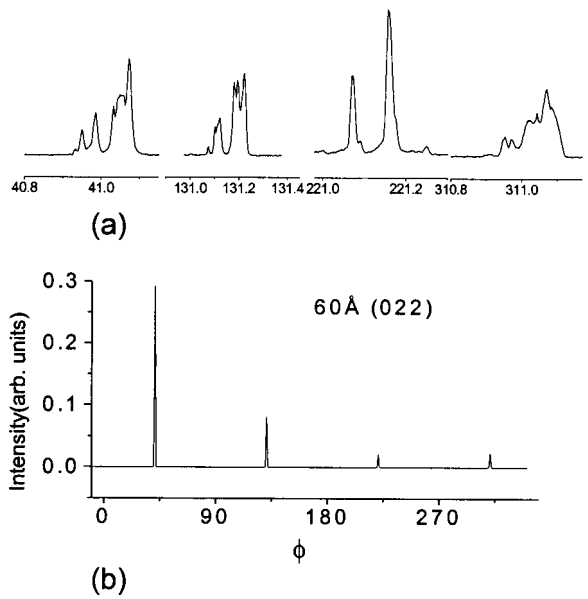

FIG. 7. ϕ scans about the (022) direction for the 60 Å film; (a) shows the expanded region near the peaks and (b) shows the full scan. No structure was found in the peaks in the 300 and 1600 Å films. However, for the 60 Å films the peaks split into multiple components as a result of small differences in orientation between crystal grains. Note that the horizontal scale in (a) is 1/15 of that in Figs. 5 and 6.

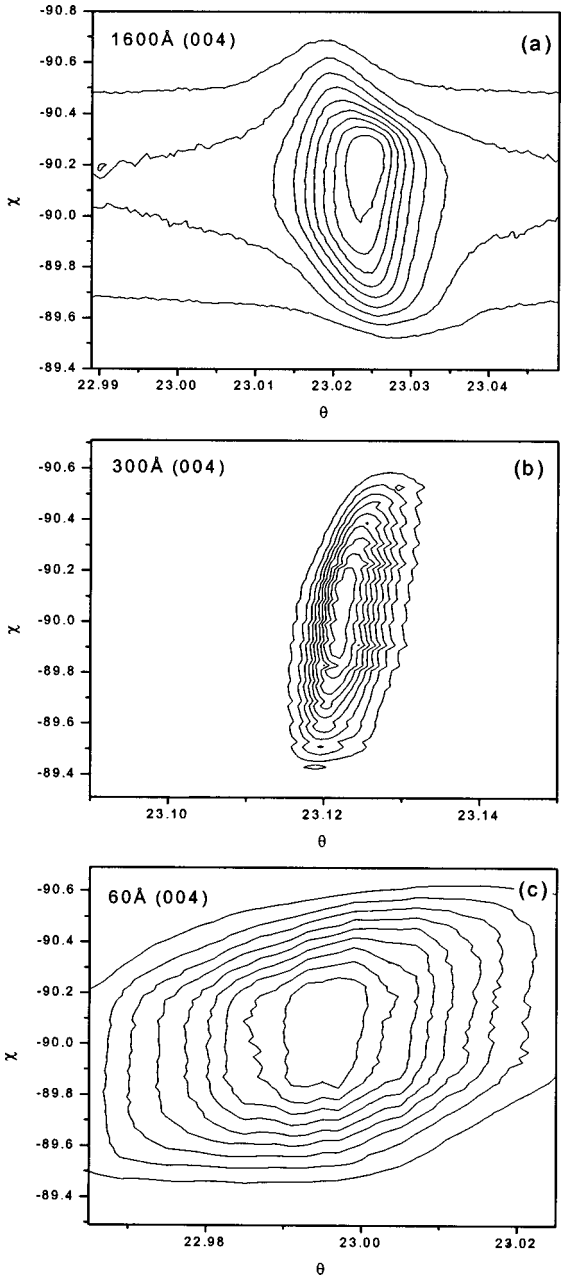

FIG. 8. $\theta-\chi$ scans of the (004) planes for the (a) 1600, (b) 300, and (c) 60 Å films. Note the narrowness of the 300 Å films indicating a high degree of crystal orientational order.

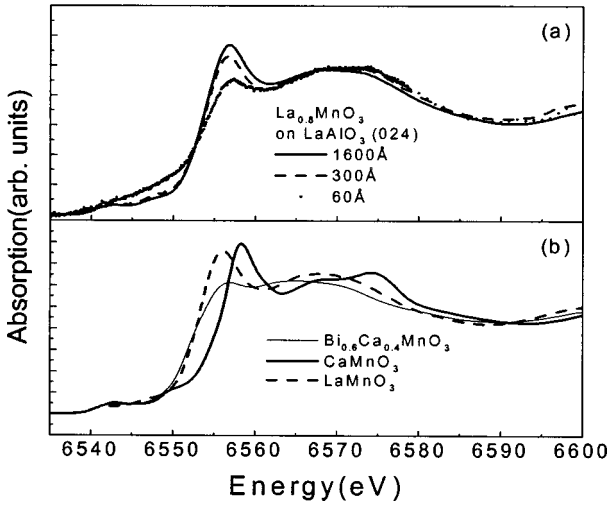

FIG. 9. (a) Near-edge x-ray absorption spectra (Mn K) of $La_{0.8}MnO_3$ films for 1600 Å (solid line), 300 Å (dashed line) and 60 Å (solid dot) films in fluorescent mode. The spectrum measured when the incidence x-ray electric field vector has 45° to the film surface. (b). XAS measurements of $Bi_{0.6}Ca_{0.4}MnO_3$, $LaMnO_3$, and $CaMnO_3$, respectively, with decreasing level of local distortions of the MnO_6 octahedra.

our recent work we have shown that in the Manganites, the local distortions are manifested by the enhancement of the width of the main line.[22,23]

In Fig. 9(b), we show as examples the spectra for $CaMnO_3$ (no JT distortions), $LaMnO_3$ [with a JT distortion and Mn–O bonds with distances of 1.907, 1.968, and 2.178 Å (Ref. 24) and $Bi_{0.6}Ca_{0.4}MnO_3$ (with large JT distortions and $Bi\,6s^2$ induced structural distortions[25]).

The important point is that the 60 Å film has very large local distortions which are significantly larger than those present in $LaMnO_3$ (see Refs. 22 and 23). Yet this film is ferromagnetic and metallic. This indicates that the film is mainly composed of a strained layer with a minor covering metallic B layer. Indeed we mention again that our magnetization measurements are consistent with ~1/2 of the volume of the 1600 Å film and ~1/4 of the 60 Å film volume being in the metallic state (assuming that only the metallic component is ferromagnetic). The behavior observed in the transport measurements suggest that the metallic region are connected.

IV. CONCLUSIONS

A study of the properties of $La_{0.8}MnO_3$ films of varying thickness was performed. Transport and magnetization measurements reveal that the metallic volume fraction of the film varies from ~1/4 for ultrathin 60 Å films to ~1/2 for 1600 Å films. We have not accounted for the possibility of a spin-canted structure, which could increase the metallic fraction of the films. Structural measurements on multiple length-scales reveal that near 300 Å, a transition (crossover region) from highly strained ultrathin films to relaxed bulk-like films occurs. The transition region is characterized by low surface roughness, high crystallite orientation, and broad *d*-spacing distributions. The two layer growth has been seen by others.[2,26,27] However, here we addressed the evolution of the relative A and B volumes with thickness on multiple length scales and commented on the volume of the ferromagnetic component.

ACKNOWLEDGMENTS

This work was supported by NSF Career Grant No. DMR-9733862 and by NSF/CNRS Project No. 9159. Data acquisition was performed at Brookhaven National Laboratory's National Synchrotron Light Source, which is funded by U.S. Department of Energy Grant No. DE-AC02-98CH10886. The AFM measurements were performed at the NJIT W. M. Keck Foundation Laboratory.

[1] Y. Tokura and Y. Tomioka, J. Magn. Magn. Mater. **200**, 1 (1999), and references therein; J. M. Coey, M. Verit, and S. von Molenar, Adv. Phys. **48**, 167 (1999), and references therein.
[2] S. Jin, T. H. Tiefel, M. McCormack, H. M. O'Bryan, L. H. Chen, R. Ramesh, and D. Schurig, Appl. Phys. Lett. **67**, 557 (1995).
[3] M. G. Blamire, B.-S. Teo, J. H. Durrell, N. D. Mathur, Z. H. Barber, J. L. McManus Driscoll, L. F. Cohen, and J. E. Evetts, J. Magn. Magn. Mater. **191**, 359 (1999).
[4] J. Z. Sun, D. W. Abraham, R. A. Rao, and C. B. Eom, Appl. Phys. Lett. **74**, 3017 (1999).
[5] Y. Suzuki, H. Y. Hwang, S.-W. Cheong, and R. B. van Dover, Appl. Phys. Lett. **71**, 140 (1997).
[6] X. W. Wu, M. S. Rzchowski, H. S. Wang, and Q. Li, Phys. Rev. B **61**, 501 (2000).
[7] H. S. Wang, Q. Li, K. Liu, and C. L. Chien, Appl. Phys. Lett. **74**, 2212 (1999); H. S. Wang and Q. Li, *ibid*. **73**, 2360 (1998).
[8] T. K. Nath, R. A. Rao, D. Lavric, C. B. Eom, L. Wu, and F. Tsui, Appl. Phys. Lett. **74**, 1615 (1999).
[9] J. O'Donnell, M. S. Rzchowski, J. N. Eckstein, and I. Bozovic, Appl. Phys. Lett. **72**, 1775 (1998).
[10] A. J. Millis, T. Darling, and A. Migliori, J. Appl. Phys. **83**, 1588 (1998).
[11] A. J. Millis *et al.* (unpublished).
[12] Z. Fang, I. V. Solovyev, and K. Terakura, Phys. Rev. Lett. **84**, 3169 (2000).
[13] J. Aarts, S. Freisem, R. Hendrikx, and H. W. Zandbergen, Appl. Phys. Lett. **72**, 2975 (1998).
[14] H. L. Ju, Kannan M. Krishnan, and D. Lederman, J. Appl. Phys. **83**, 7073 (1998).
[15] S. Pignard, H. Vincent, J. P. Sénateur, and J. Pierre, J. Magn. Magn. Mater. **177-181**, 1227 (1998).
[16] Q. Qian, T. A. Tyson, C. Dubourdieu, A. Bosak, J. P. Sénateur, M. Deleon, J. Bai, and G. Bonfait, Appl. Phys. Lett. **80**, 2663 (2002).
[17] A. Bossak, C. Dubourdieu, M. Audier, J.P. Sénateur, J. Pierre, O. Gorbenko, and A. Kaul (unpublished).
[18] J. P. Sénateur, R. Madar, F. Weiss, O. Thomas, and A. Abrutis, French Patent No. FR270671 (7/12/1993); European Patent No. EP0730671 (7/8/1994); US Patent No. US5945162 (8/31/1999).
[19] F. Felten, J. P. Senateur, F. Weiss, R. Madar, and A. Abrutis, J. Phys. IV **C5**, 1079 (1995); C. Dubourdieu, M. Audier, J. P. Sénateur, and J. Pierre, J. Appl. Phys. **86**, 6945 (1999).
[20] A. Gupta, T. R. McGuire, P. R. Duncombe, M. Rupp, J. Z. Sun, W. J. Galleger, and G. Xiao, Appl. Phys. Lett. **67**, 3494 (1995).
[21] S. Pignard, H. Vincent, J. P. Sénateur, J. Pierre, and A. Abrutis, J. Appl. Phys. **82**, 4445 (1997).
[22] Q. Qian, T. A. Tyson, C.-C. Kao, W. Prellier, J. Bai, A. Biswas, and R. L. Greene, Phys. Rev. B **63**, 224424 (2001).
[23] Q. Qian, T. A. Tyson, C.-C. Kao, M. Croft, S.-W. Cheong, G. Popov, and M. Greenblatt, Phys. Rev. B **64**, 024430 (2001).
[24] J. Rodriguez-Carvajal, M. Hennion, F. Moussa, A. H. Moudden, L. Pinsard, and A. Revcolevschi, Phys. Rev. B **57**, R3189 (1998).
[25] H. Woo, T. A. Tyson, M. Croft, S.-W. Cheong, and J. C. Woicik, Phys. Rev. B **63**, 134412 (2001).
[26] (a) W. Prellier, A. Biswas, M. Rajeswari, T. Venkatesan, and R. L. Greene, Appl. Phys. Lett. **75**, 397 (1999); (b) A. Biswas, M. Rajeswari, R. C. Srivastava, Y. H. Li, T. Venkatesan, R. L. Greene, and A. J. Millis, Phys. Rev. B **61**, 9665 (2000).
[27] F. Pailloux, R. Lyonnet, J.L. Maurice, and J.P. Contour, Appl. Surf. Sci. **177**, 263 (2001).